JOURNAL OF SOLID STATE CHEMISTRY **131,** 9–17 (1997)
ARTICLE NO. SC977268

Ferroelectric Tungsten Trioxide

P. M. Woodward and A. W. Sleight[1]

Department of Chemistry and Center for Advanced Materials Research, Oregon State University, Corvallis, Oregon 97331-4003

and

T. Vogt

Department of Physics, Brookhaven National Laboratory, Upton, New York 11973

Received October 29, 1996; accepted December 19, 1996

The structure of a low-temperature form of tungsten trioxide, ε-WO_3, has been determined for the first time. Earlier inconclusive evidence for ferroelectricity in this form is confirmed. There are at least six forms of WO_3, but ε-WO_3 is the only form now shown to be acentric. The structure analysis of ε-WO_3 was based primarily on Rietveld analysis of high-resolution neutron diffraction data obtained at 15 K. Higher resolution synchrotron X-ray diffraction data were used to confirm the space group. This ε-form of WO_3 is monoclinic with a space group of Pc, $a = 5.278$ Å, $b = 5.156$ Å, $c = 7.664$ Å, $\beta = 91.762^\circ$, and $Z = 4$. During the transformation from triclinic δ-WO_3 to the monoclinic ε-WO_3, no change in the octahedral tilt system occurs, but there are significant shifts in the W atom positions. These W atom shifts result in an enhancement of the long–short bond distance alternation in the [110] direction (the [100] direction of the δ-phase), which is related to changes in electrical and optical properties.

INTRODUCTION

The structure of WO_3 is best described as a three-dimensional network of corner-sharing WO_6 octahedra. The connectivity of this network is identical to the cubic ReO_3 structure and the AMO_3 perovskite structure in the absence of an A cation. However, the symmetry of WO_3 is lowered from the ideal ReO_3 structure by two distortions: tilting of WO_6 octahedra and displacement of tungsten from the center of its octahedron. Variations in the details of these distortions give rise to several phase transitions. In fact tungsten trioxide adopts at least five distinct crystallographic modifications between absolute zero and its melting point at 1700 K (1, 2). When the temperature is decreased from the melting point, the crystallographic symmetry for WO_3 changes in the sequence: tetragonal–orthorhombic–monoclinic–triclinic–monoclinic. Most of the transitions appear to be first order, and they often display large hysteresis in the transition temperature (1, 2). A summary of these transitions is given in Table 1. Additionally DTA, heat capacity (3, 4), and resistivity (5) studies show discontinuities indicative of phase transitions at approximately 1170 and 1500 K. Furthermore, capacitance and electrical resistivity measurements suggest phase transitions in the low-temperature region at 40, 65, and 130 K (6). However, structural refinements have not previously been performed in the necessary temperature intervals to determine if these discontinuities in the physical properties actually correspond to structural phase transitions of WO_3.

Tanisaki observed a small broad endothermic peak in the DTA curve and a slight decrease in the electrical resistivity (from 0.7 to 0.4 Ω-cm) upon heating crystals through the δ-WO_3 to γ-WO_3 phase transition near 290 K (7). Salje and Viswanathan found the resistivity to decrease from approximately 2.0 to 0.2 W-cm upon heating from 293 to 1123 K (1). The optical band gap (2.58 eV at room temperature) is found to gradually decrease and become increasingly diffuse as the temperature is raised to 773 K (8).

More significant changes in WO_3 properties are reported upon cooling through the δ-to-ε phase transition at $\cong$ 230 K. An abrupt 20-to-30-fold increase in the resistivity occurs at this transition (1, 7). The optical band gap increases from 2.6 eV to an unknown value > 2.85 eV, resulting in a color change from pale green to bluish-white (1). Tanisaki observed a sharp exothermic peak in the DTA curve (endothermic upon heating) and a rather large volume contraction ($\cong 1\%$) upon cooling through the transition temperature (7). Salje and Viswanathan observed the onset of piezoelectricity upon transformation to the ε-phase (1). Hysteresis loops in the dielectric behavior at low temperatures

[1] To whom correspondence should be addressed.

0022-4596/97 $25.00

TABLE 1
Known Polymorphs of Tungsten Trioxide

Phase	Symmetry	Space group	Z	Temperature range (K)[a]	Reference
α-WO_3	Tetragonal	$P4/nmm$	2	1010–1170	Kehl *et al.* (31)
β-WO_3	Orthorhombic	$Pmnb$	8	600–1170	Salje (32)
γ-WO_3	Monoclinic	$P2_1/n$	8	290–600	Tanisaki (33) Loopstra and Rietveld (34)
δ-WO_3	Triclinic	$P\bar{1}$	8	230–290	Diehl *et al.* (35) Woodward *et al.* (14)
ε-WO_3	Monoclinic	Pc	4	0–230	Salje (13)

[a] The transition temperatures display large hysteresis effects and universal agreement is not found in the literature. They are taken primarily from references 1, 2, 7, and 35.

have been observed in sintered pellets and crystals of WO_3 suggesting the presence of ferroelectricity (6, 9, 10). When ε-WO_3 was intentionally reduced to introduce more charge carriers, the electrical transport was found to be highly anisotropic ($\sigma_{ab}/\sigma_c > 100$) (11). Furthermore, if the measurements are performed in the dark, bipolaronic transport is reported (11, 12). Clearly the physical properties of the ε-phase are distinctly different from the properties of the other four WO_3 polymorphs; ε-WO_3 might well be viewed as the most interesting form of tungsten trioxide.

The structure of ε-WO_3 is the least accurately known of all of the WO_3 polymorphs. The lattice constants were first determined by Tanisaki in 1960 (7). Sixteen years later, Salje determined approximate tungsten positions but made no attempt to determine oxygen positions because the crystal used became highly twinned upon cooling through the δ-to-ε phase transition (13). The large volume contraction associated with the phase transition and the high degree of pseudosymmetry in the ε-phase make it nearly impossible to obtain good quality, untwinned single crystal of ε-WO_3. Salje also looked at powdered WO_3 samples but did pursue this route because the samples used showed incomplete and sometimes almost no transition to the ε-phase even at 133 K (13). With the advances made in powder diffraction over the past 20 years, it seemed appropriate to revisit the structure of ε-WO_3.

EXPERIMENTAL

The sample used in this experiment was the same sample that was used for an earlier investigation of δ-WO_3. Experimental details of its preparation are given elsewhere (14). Data collection was performed on the high-resolution neutron powder diffractometer (HRNPD) at beamline H1A of the high flux beam reactor (HFBR) at Brookhaven National Laboratory (BNL). The experimental details of this diffractometer have been described previously (14). Low-temperature spectra were collected using a two-stage Air Products displex for temperature control. Upon cooling, a data set was collected at 200 and 15 K. After the data collection at 15 K was complete, spectra were recorded upon warming at 50, 100, 150, and 200 K. The multibank detector array was moved in 0.02° steps for the 15 and 200 K data sets collected on cooling and in 0.05° steps for the data sets collected on warming. Integration times for all runs were roughly 5 min per step.

Low-temperature X-ray diffraction measurements were performed at 20 and 50 K at beamline X7A of the National Synchrotron Light Source (NSLS) at BNL. The sample was cooled in a two-stage Air Products displex using flat plate geometry. A point detector was used, and due to the sharpness of the lines a step size of 0.003° was chosen. The sample was rocked about the theta position to reduce preferred orientation. To obtain a highly monochromatic beam, the incoming beam was passed through a Ge(111)–Ge(220) crystal analyzer. The X7A experimental arrangement is discussed in greater detail elsewhere (15).

STRUCTURE REFINEMENT

Initially, a neutron powder diffraction pattern was obtained at 200 K. However, inspection of this pattern revealed at least two phases of WO_3 in significant quantities. With the goal of obtaining a single phase pattern, another diffraction pattern was collected at 15 K. This pattern appeared to be single phase, although subsequent refinements showed the presence of a small amount of another WO_3 phase. The second phase had lattice constants similar to δ-WO_3, but the peaks were too weak for complete structural analysis. With the exception of the very weak second phase peaks, all of the reflections in the 15 K pattern could be indexed using the lattice constants reported for ε-WO_3 in the literature (7, 13). At this point the peak intensities were extracted using the program EXTRA (16). The EXTRA software package fits the entire pattern beginning from the space group and lattice constants, and extracts the intensity

of each peak using the LeBail method (17). The extracted peak intensities were then used as input for the direct methods program SIRPOW (18), and all eight atoms of the asymmetric unit were located with an $R(F)$ of 7.18% and an $R(F^2)$ of 9.99%. The atomic positions from SIRPOW were then used as the starting point for a Rietveld refinement using the program GSAS (19). After addition to the refinement of δ-WO_3 as a second phase, the refinement quickly converged to the structure given in Table 2. The observed and difference patterns are shown in Fig. 1. Selected bond distances and angles are given in Table 3. Because of the very weak intensity of even the strongest δ-WO_3 peaks, only the lattice constants and phase fraction of this minority phase were refined. The profile coefficients and thermal parameters were fixed at the values obtained for the ε-phase, and the atomic positions were constrained to the atomic positions previously determined (14). This procedure was found to adequately account for all peaks not associated with ε-WO_3.

Refinements were also carried out in space group $P1$, using the monoclinic structure as a starting model. The R_{wp} factor was found to drop from 9.92 to 9.74%. Applying the Hamilton significance test (19) indicates that even at the 50% confidence level, the triclinic refinement is not statistically better than the monoclinic refinement. Furthermore, neither α nor γ refines significantly away from 90°, nor does any one peak or region of the spectrum fit significantly better in the triclinic refinement. From these observations, we conclude that the true symmetry is monoclinic, space group Pc. This is in agreement with Salje's findings based on photographs of twinned single crystals (13).

TABLE 2
Final Results of the GSAS Structural Refinement of the 15 K Neutron Diffraction Pattern

Space Group	Pc	a(Å)	5.27793(3)
R_{wp} (%)	9.91	b(Å)	5.15594(3)
R_p (%)	7.53	c(Å)	7.66392(4)
χ^2	2.22	α(°)	90
$R(F^2)$ (%)	6.13	β(°)	91.762
$R(F)$ (%)	4.31	γ(°)	90
Number of reflections	237	Volume (Å^3)	208.45
Number of variables	44	Zero	0.0904(5)

Atom	x	y	z	U_{iso}
W1	− 0.004(2)	− 0.014(1)	− 0.0218(2)	− 0.0012(4)
W2	0.508(2)	0.472(1)	0.0550(2)	− 0.0012
O3	0.213(1)	0.708(1)	− 0.013(1)	0.0005(2)
O4	0.285(1)	0.215(1)	0.063(1)	0.0005
O5	0.7086(7)	0.791(1)	− 0.023(1)	0.0005
O6	0.795	0.290(1)	0.057(1)	0.0005
O7	− 0.004(2)	0.0717(9)	0.764(1)	0.0005
O8	0.501(2)	0.4201(9)	0.778(1)	0.0005

Based on capacitance and resistivity discontinuities Lefkowitz, Dowell, and Shields suggested that below room temperature WO_3 undergoes phase transitions at 40, 65, 130, 220, and 260 K. The latter two transitions appear to correspond to the γ-to-δ and δ-to-ε phase transitions,

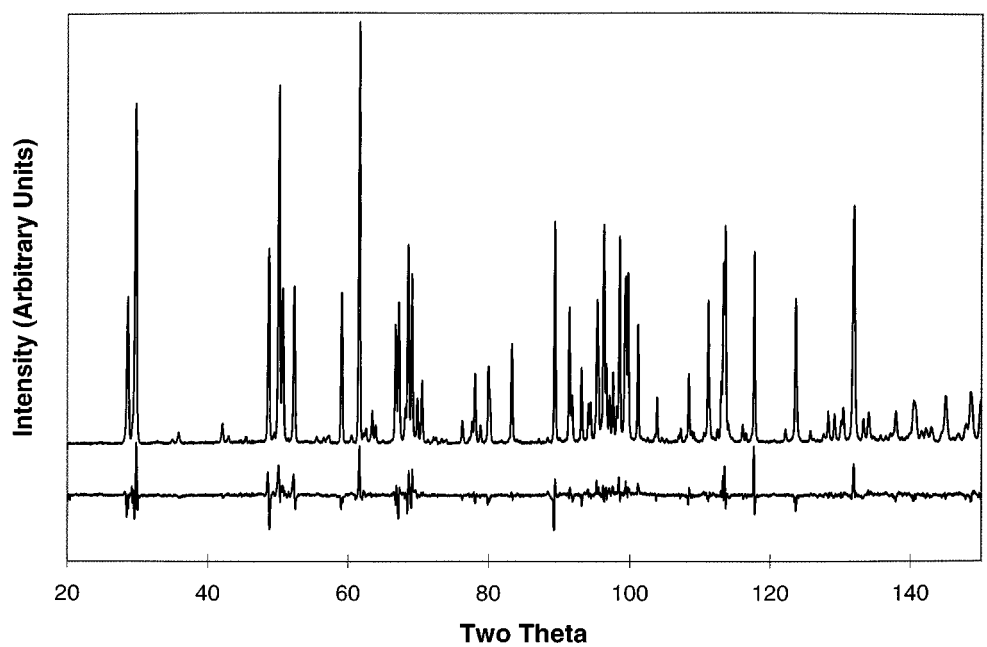

FIG. 1. The observed, calculated, and difference patterns for the final GSAS refinement of the 15 K neutron diffraction pattern.

TABLE 3
Selected Bond Distances (Å) and Angles (°) for WO_3 at 15 K

W1–O3	1.840(6)	W2–O3	2.028(10)
W1–O4	2.022(10)	W2–O4	1.775(8)
W1–O5	1.819(10)	W2–O5	2.053(7)
W1–O6	1.994(7)	W2–O6	1.782(10)
W1–O7	1.700(9)	W2–O8	2.140(11)
W1–O7	2.210(10)	W2–O8	1.797(10)
W1–O3–W2	161.7(6)		
W1–O4–W2	156.9(5)		
W1–O5–W2	151.5(6)		
W1–O6–W2	150.6(6)		
W1–O7–W1	157.2(3)		
W2–O8–W2	154.7(3)		

respectively, but the first three temperatures suggest phase transitions which have not been otherwise observed. To look for such transitions, neutron diffraction patterns were collected at 50, 100, and 150 K upon warming from 15 K. An inspection of the patterns showed them all to be very similar. No abrupt change in the patterns is observed, suggesting no phase transition exists between 15 and 150 K. This is consistent with the absence of discontinuities in the dc conductivity measurements (11). Nonetheless, all of the patterns were refined to look for subtle changes in the structure. Table 4 contains a summary of these refinements. Figure 2 shows the changes in the cell dimensions of ε-WO_3 as temperature is varied.

Low-temperature synchrotron X-ray data sets were collected at 20, 50, 100, 150, 200, and 250 K. Preferred orientation effects were pronounced; therefore, these data were unsuitable for structure refinement. However from the peak positions, there are important conclusions. First, no peak splitting in addition to that found in the neutron patterns is observed, and all peaks can be indexed with the unit cell described in Table 2. This adds further weight to the conclusion that *Pc* is the correct space group, as suggested in the literature (13) and deduced from this neutron diffraction study. Second, the minority WO_3 phase which appears in the neutron diffraction pattern is also clearly visible in the X-ray diffraction pattern, and the lattice constants of this phase are seen to smoothly evolve from those of the δ-phase at higher temperatures.

Upon cooling our WO_3 sample to 200 K, a multiphase neutron diffraction pattern was obtained. Attempts to refine this pattern as a two-phase mixture of δ-WO_3 and ε-WO_3 did not succeed in accurately fitting the pattern. Upon warming from low temperature, the peak intensities of the minority phase noticeably increase at 200 K, even though this is apparently below the ε-to-δ phase transition temperature. The X-ray diffraction patterns obtained at 200 K and below always showed at least two (possibly more) phases of WO_3. A more thorough study is in progress using both X-ray and neutron diffraction to determine if there really is another WO_3 phase at low temperatures in addition to δ-WO_3 and ε-WO_3.

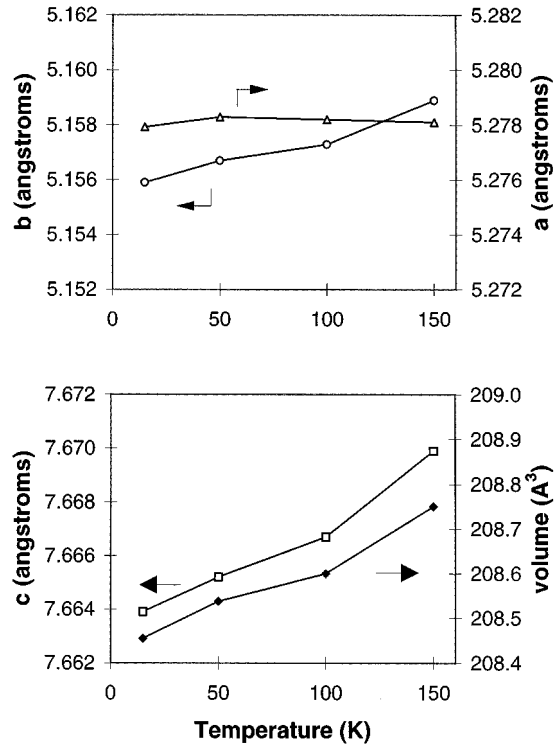

FIG. 2. The (a) *a* lattice constant, (b) *b* lattice constant, (c) *c* lattice constant, and (d) unit cell volume of ε-WO_3 as a function of temperature.

TABLE 4
Partial Refinement Results for Neutron Data Sets Collected upon Warming from 15 K[a]

Parameter	50 K	100 K	150 K
R_{wp} (%)	11.04	10.87	13.03
R_p (%)	8.38	8.18	10.03
χ^2	4.11	4.03	5.77
a (Å)	5.27829(8)	5.27821(5)	5.2781(1)
b (Å)	5.15666(8)	5.15728(5)	5.1589(1)
c (Å)	7.6652(1)	7.66669(7)	7.6699(1)
β (°)	91.758(1)	91.750(1)	91.727(2)
Volume (Å^3)	208.54	208.60	208.75
Minority phase fraction (%)	2.7	2.4	4.2
Tungsten U_{iso}	0.0026(6)	0.0032(6)	0.0046(8)
Oxygen U_{iso}	0.0062(4)	0.0061(3)	0.0082(5)

[a] The detector step size was 0.05° 2θ rather than 0.02° 2θ used for the 15 K data set. The difference in step size is partially responsible for the higher values of R_{wp} observed in these samples.

DISCUSSION

As WO_3 is cooled from high temperatures, it undergoes several phase transitions; usually the symmetry is lowered at each phase transition occurring with decreasing temperature. In contrast, the δ-to-ε transition might be regarded as a phase transition with increasing symmetry because it is a triclinic-to-monoclinic transition with the unit cell becoming smaller and with the introduction of a glide plane. However, the δ-to-ε transition is centric-to-acentric; thus, from this point of view symmetry is lowered.

Both tilting of the oxygen octahedra and displacement of tungsten from the center of those octahedra are responsible for lowering the symmetry of WO_3 from the cubic ReO_3 structure. Changes in either or both of these distortions are responsible for all of the phase transitions in WO_3. Upon cooling from high-temperature tetragonal α-WO_3 to triclinic δ-WO_3, a change in the octahedral tilt system (21, 22) accompanies each of the phase transitions. The easiest way to observe such a change in tilt system is to view a polyhedral representation of the structure down each of the three directions along which the octahedra share corners. Figure 3 shows such a view of the ε-WO_3 structure. One can readily see that octahedral tilting is out-of-phase down each of the three Cartesian axes. Neglecting the magnitudes of the tilts this corresponds to the $a^-b^-c^-$ Glazer tilt system, which is also observed in δ-WO_3 (14). Therefore, unlike the other phase transitions of WO_3, no change in the tilt pattern occurs at the δ-to-ε phase transition.

To further examine the structural differences between δ and ε phases, the structure of ε-phase was first constructed in large ($Z = 8$) cell analogous to δ-WO_3. Next the symmetry of each structure was reduced to $P1$ and the program IVTON (23) was used to determine the volume center of each octahedron. Also, the direction and magnitude of each tungsten ion shift with respect to the octahedral center of volume was determined. Table 5 lists the positions of the center of volume for each of the eight octahedra present in the large cell. For ease of comparison the positions are given in actual distances rather than fractional coordinates. A Cartesian coordinate system is used, and both structures have been shifted so that the origin is located at the volume center of the first octahedron. The tilting sense of this octahedron is the same in both structures. The fact that only very small differences are observed between the two structures confirms that the oxygen ion positions do not change significantly through the phase transition.

If a change in the octahedral tilting arrangement does not drive the δ-to-ε transition, as it does the γ-to-δ transition (14), then shifts in the tungsten positions must be the driving force for the phase transition. The tungsten shifts, for the octahedra contained in Table 5, are tabulated in Table 6 and shown in Figs. 4 and 5. One can immediately see that the tungsten positions have changed significantly upon transformation to the ε-phase. To describe the differences between the two structures, it is most convenient to decompose the structure into one-dimensional W–O chains running roughly parallel to each of the three Cartesian axes. The chains of course intersect at the tungsten ions to give

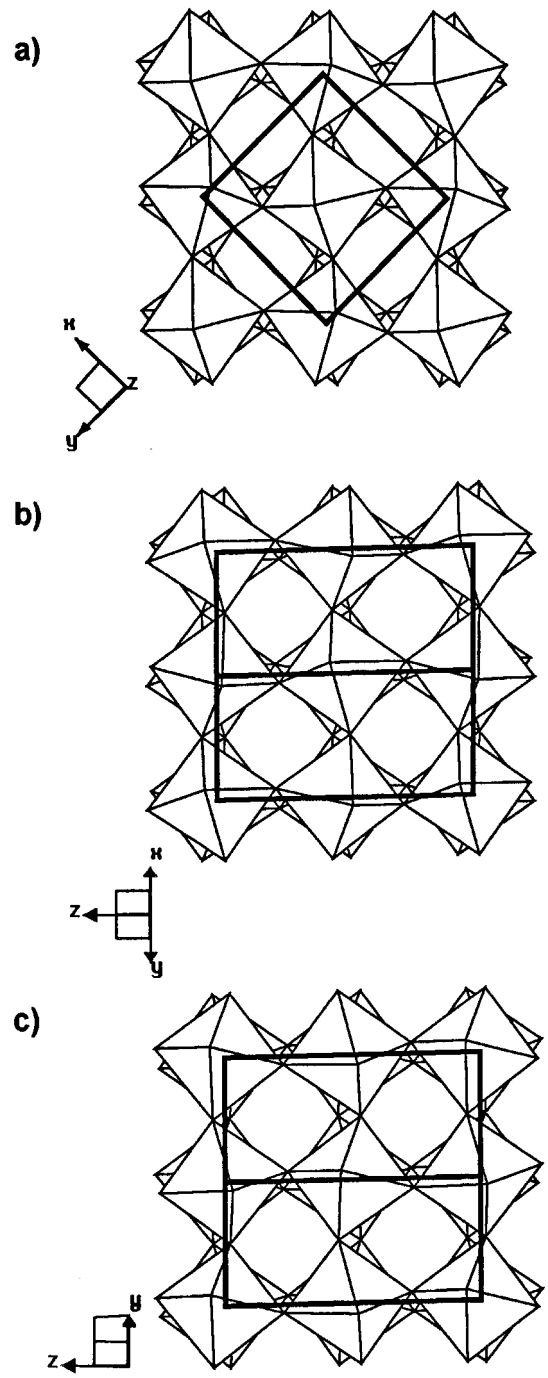

FIG. 3. A polyhedral representation of the ε-WO_3 structure looking down the (a) [001] direction, (b) [$\bar{1}$10] direction, and (c) [110] direction. The bold lines represent the unit cell.

TABLE 5
The Cartesian Coordinates (Å) of the Volume Centers of the Eight WO_6 Octahedra Present in the Large Cell ($Z = 8$)[a]

	Delta phase			Eta phase			
Octahedron	x	y	z	x	y	z	Distance
1	0.000	0.000	0.000	0.000	0.000	0.000	0.000
2	− 0.064	3.765	− 0.022	− 0.078	3.678	0.118	0.165
3	3.665	− 0.111	− 0.090	3.694	− 0.006	− 0.045	0.118
4	3.609	3.650	− 0.053	3.603	3.687	0.000	0.065
5	− 0.005	− 0.005	3.837	0.006	0.006	3.832	0.016
6	− 0.072	3.755	3.821	− 0.069	3.685	3.787	0.078
7	3.660	− 0.116	3.746	3.700	0.000	3.787	0.129
8	3.601	3.640	3.788	3.609	3.693	3.832	0.069

[a] These values were calculated with the program IVTON (23) and shifted so that the origin in each structure corresponds to the volume center of the first octahedron.

the three-dimensional structure. By examining the direction and magnitude of the tungsten shifts in each chain, the structures can be qualitatively described.

The most striking differences between the two structures can be found in the xy plane. Beginning with the δ-phase, the tungsten ions show an average shift of 0.17 Å in the y direction, but only a 0.03 Å shift in the x direction. This gives rise to a much more pronounced long–short bond alternation in the y direction, as shown in Figs. 4a and 4b. Furthermore, in each xy plane the shifts in the y direction are in opposite directions in neighboring chains. This results in a long–short bond alternation in each chain which is out-of-phase with bond alternation in both neighboring chains. In the x direction the shifts, although much smaller, are in the same direction in neighboring chains, resulting in an in-phase relationship within the xy plane. The shifts in the layer immediately above (and below), shown in Fig. 4b, can be derived from the inversion center at the center of the eight W atoms of Figs. 4a and 4b.

Examining now the ε-phase, there are two important differences between it and the δ-phase. First, the magnitude of the shifts has increased in the x direction and decreased in the y direction, so that the two are now comparable. This enhances the long–short bond alternation in the x direction and has important consequences on the physical properties. This will be later discussed in more detail. The second obvious difference between δ and ε phases is the direction of the shifts in the y direction. In the ε-phase all of the y direction shifts within a single xy plane are in the same direction. This gives in-phase long–short bond alternation in both x and y directions, as shown in Fig. 4c. However, as shown in Fig. 4d the c glide plane causes the tungsten ions in neighboring xy planes to shift in the opposite direction. This results in an overall net shift of zero in both the x and y directions (see Table 6).

Comparing the tungsten shifts in the z direction (Fig. 5), one finds that shift directions are the same for both structures. Each chain that runs in the z direction has two neighboring chains in the x direction and two neighboring chains in the y direction. If the tungstens shift in the positive z direction in the central chain, then the tungsten shifts in all four neighboring chains will be in the opposite direction. This results in an out-of-phase relationship in the long–short bond alternation between the central chain and all four of the neighboring chains. This relationship is common to both structures. However if the magnitude of the shifts are carefully examined, differences between the two structures are revealed. Whereas in the δ-phase the magnitude of the shifts in the z direction are all roughly the same, in the ε-phase the shifts in the negative z direction are larger than those in the positive z direction. Because of the inequality of shifts in the z direction, a net spontaneous polarization develops along the c axis of the ε-phase. Similarly, a net

TABLE 6
The Cartesian Coordinates (Å) of the Tungsten Shifts (with Respect to the Octahedral Volume Centers)[a]

	Delta phase			Eta phase		
Octahedron	x	y	z	x	y	z
1	0.050	0.136	0.248	0.035	0.081	−0.321
2	0.007	0.148	−0.252	0.088	0.112	0.227
3	0.037	−0.180	−0.230	0.088	0.112	0.227
4	−0.012	−0.201	0.225	0.035	0.081	−0.321
5	−0.037	0.180	0.230	−0.035	−0.081	−0.321
6	0.012	0.201	−0.225	−0.088	−0.112	0.227
7	−0.050	−0.136	−0.248	−0.088	−0.112	0.227
8	−0.007	−0.148	0.252	−0.035	−0.081	−0.321
Net shift	0	0	0	0	0	−0.376
Average shift	0.027	0.166	0.239	0.062	0.097	0.274

[a] For the set of octahedra listed in Table 5. These values were calculated with the program IVTON (23).

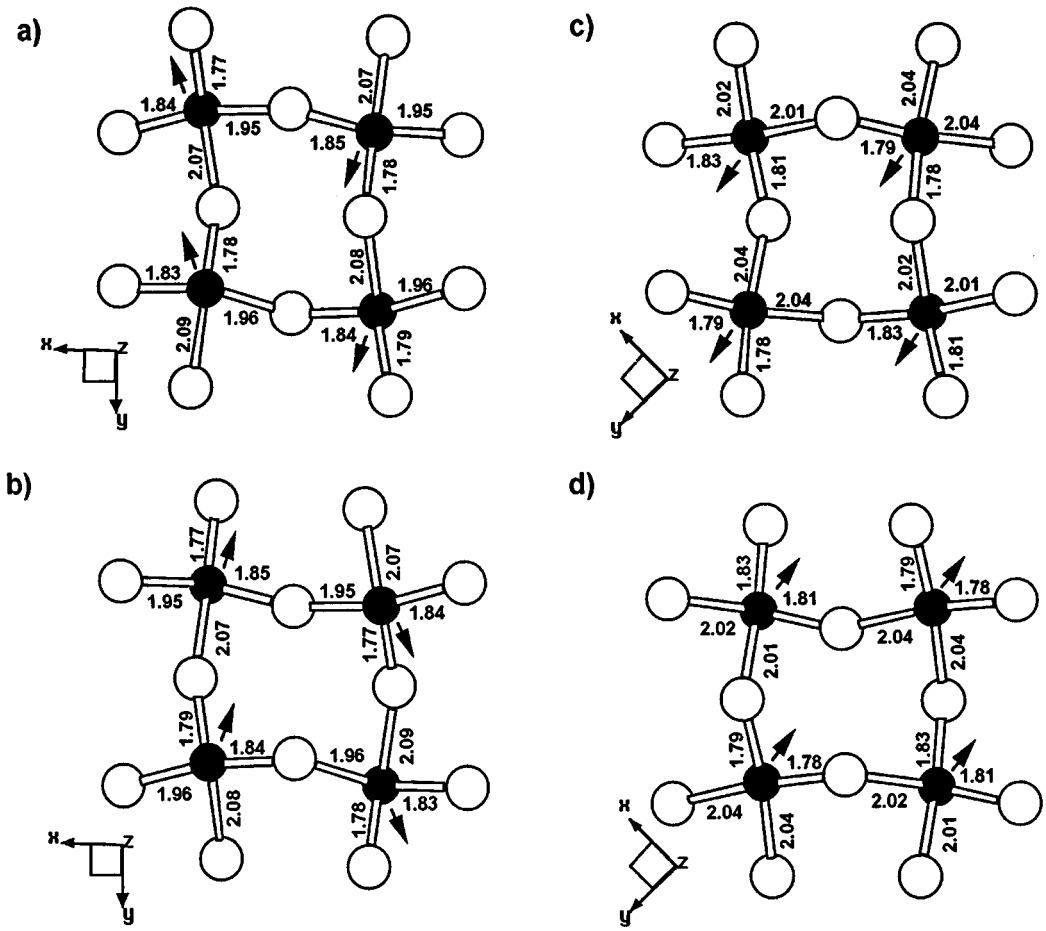

FIG. 4. A view of the tungsten oxygen linkages in the (001) layers in δ-WO_3 with (a) $z \cong 0.25$, (b) $z \cong 0.75$, and ε-WO_3 with (c) $z \cong 0.25$, and (d) $z \cong 0.75$. The dark circles represent tungsten, while the open circles represent oxygen. The arrows indicate the direction of the tungsten shifts, and the bond distances in angstroms are listed next to each bond.

spontaneous polarization develops along the a axis of the ε-WO_3 unit cell. However, based on the shifts of the W ions, the magnitude of the polarization is larger in the z direction than it is in the x direction. (Also note that apparently no net polarization develops in the [110] and [$\bar{1}$10] directions, which correspond to the [100] directions of the larger σ-WO_3 cell.) The presence of an inversion center precludes net polarization in δ-WO_3. In ε-WO_3 the presence of a net polarization perpendicular to the b axis explains the observance of hysteresis loops in the dielectric behavior of WO_3 at low temperatures (6, 9). The fact that the tungsten shifts partially cancel each other may also help to explain why the hysteresis signal is weak and difficult to observe reproducibly.

A volume contraction occurs upon transformation into the ε-phase. The contraction could occur as a result of compression of the WO_6 octahedra or it could be realized by increased tilting of the octahedra. Table 7 contains a summary of the main structural features of the γ, δ, and ε phases. These results suggest that increased octahedral tilting is mainly responsible for the decreased volume of the ε-phase.

Considering the room temperature band gaps of γ- and δ-WO_3 and the fact that W^{VI} is d^0, we expect a light yellow color for these forms of WO_3. This color is due to an oxygen-to-tungsten charge transfer transition (valence band to conduction band transition) which is mainly in the UV but has a tail into the visible spectrum. The fact that samples of these materials are most frequently found to be light green is caused by an additional light blue component to the optical absorption. The light blue component is due to a W^{V}-to-W^{VI} electron transfer caused by the fact that WO_3 samples are slightly oxygen deficient. Annealing WO_3 at high temperatures, even under an atmosphere of pure oxygen, inevitably causes some loss of oxygen. The oxygen deficiency tends to be present at extended defects rather than as point defects. Obtaining stoichiometric WO_3 by annealing at low temperatures is extremely difficult because

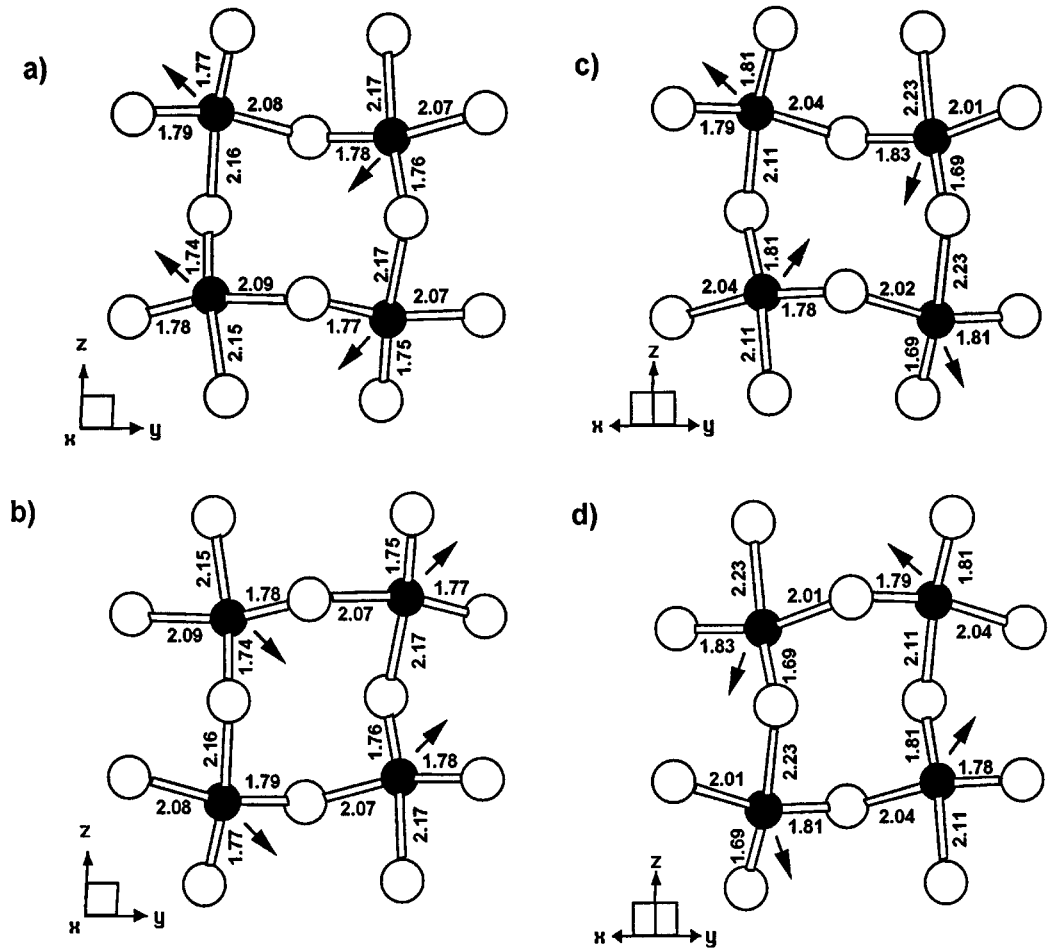

FIG. 5. A view of the tungsten oxygen linkages in the (100) layers of δ-WO_3 with (a) $x \cong 0.75$, (b) $x \cong 0.25$, and the (110) layers of ε-WO_3 passing through (c) 0.5, 0.5, z, and (d) 0, 0, z. The dark circles represent tungsten, and the open circles represent oxygen. The arrows indicate the direction of the tungsten shifts, and the bond distances in angstroms are listed next to each bond.

these extended defects are difficult to completely destroy. The W^V present in WO_{3-x} is the source of electron carriers in pure material. The oxygen deficiency and associated extended defects, inevitably present, impact color and electrical properties. They may also affect the phase transitions.

Band gaps normally decrease with increasing temperature because there is some coupling between the electronic transition responsible and the atomic vibrations. For example, many yellow materials are observed to become red on warming. This is a completely reversible transition. Likewise, cooling a light yellow material can cause a material to become colorless as the band gap naturally increases. In the case of WO_3, the color at low temperatures was described as bluish white. The yellow component has disappeared due to a band gap shift, but the blue component remains due to the slight reduction of the sample. A pronounced and abrupt decrease in the optical band gap is reported for WO_3 at the δ-to-ε phase transition. Tungstates based on tetrahedral W have larger band gaps than tungstates based on octahedral W with the associated longer W–O distances. By analogy, the higher band gap of ε-WO_3 relative to δ-WO_3 is likely related to a small but significant decrease in the average W–O distance for the three shortest such distances.

Although all the phase transitions of WO_3 may be described as displacive rather than reconstructive, they tend to be first order rather than second order. Both the γ-to-ε and δ-to-ε transitions are clearly first order. Large hysteresis effects are observed. Two or more forms of WO_3 are commonly observed to coexist. The γ-to-δ transition is well documented to be sluggish. Near the phase transition it is not unusual for both phases to be present simultaneously in either crystals (1, 7) or powders (14). However, the temperature range over which both γ and δ phases have been simultaneously observed is much smaller than the two-phase temperature range we observe for the coexistence of the δ and ε phases. This is not surprising because there is less available thermal energy at lower temperatures to overcome the activation barrier of a first-order phase transition.

TABLE 7
Summary of the Main Structural Features of the γ, δ, and ε Phases of WO_3

	γ-phase	δ-phase	ε-phase
a (Å)	7.306	7.309	7.378
b (Å)	7.540	7.522	7.378
c (Å)	7.692	7.686	7.664
a (°)	90.00	89.85	88.73
b (°)	90.88	90.91	91.27
g (°)	90.00	90.94	91.34
Volume (Å^3)	423.7	422.5	417.0
Average octahedral volume (Å^3)	9.30	9.30	9.32
Tilt system	$a^-b^+c^-$	$a^-b^-c^-$	$a^-b^-c^-$
Average tilt angle (°)			
x	156	156	154
y	159	159	155
z	161	160	157
Average W–O distance (Å)			
x	1.86/1.94	1.84/1.96	1.80/2.03
y	1.76/2.11	1.78/2.08	1.80/2.03
z	1.74/2.18	1.75/2.16	1.75/2.17

[a] The ε-phase has been converted to the large ($Z = 8$) cell for comparison with the other two polymorphs.

Particle size, impurities, and nonstoichiometry of WO_{3-x} may all influence the transition temperature of individual crystallites. Through addition of niobium Roth and Waring were apparently able to stabilize the ε-phase up to 1010 K, where it transformed directly to the α-phase (29). Berak and Sienko found that the presence of oxygen vacancies decreased both the γ-to-δ and δ-to-ε phase transition temperature (30). It is thus apparent that the transition temperatures can be significantly altered by small changes in the composition. As alluded to earlier, the possibility of another phase existing in the intermediate temperature range (150–220 K) may also help explain this behavior. The second phase present in the low-temperature diffraction patterns may well be a new phase of WO_3 rather than δ-WO_3, and the transition temperature for transformation from this unknown phase to ε-WO_3 could be much lower than 220 K. Further work is necessary to resolve these questions. The complicated situation with regard to phases present in WO_3 at low temperatures complicates the interpretation of reported physical properties of WO_3 as a function of temperature. Such studies in the literature have not been coupled with good structural studies as a function of temperature. Thus, they may be quite misleading.

ACKNOWLEDGMENTS

The neutron diffraction data were collected at the high flux beam reactor at Brookhaven National Laboratory which is supported by the Division of Materials Sciences, U.S. Department of Energy under Contract DE-AC02-76CH0016. The synchrotron data were collected at the National Synchrotron light source at Brookhaven National Laboratory, which is also supported by the Division of Materials Sciences and the Division of Chemical Sciences. Thanks to Dave Cox for assistance and advice in collection of the synchrotron data. Both the EXTRA/SIRPOW and IVTON software packages were instrumental in determining and analyzing the crystal structure. The authors express their gratitude to the authors of both software packages for access to their programs.

REFERENCES

1. E. Salje and K. Viswanathan, *Acta Crystallogr. A* **31,** 356–359 (1975).
2. C. N. R. Rao and B. V. S. Rao, *Natl. Stand. Ref. Data Ser. Natl. Bur. Stand.* **49,** 117–122 (1974).
3. C. Rosen, E. Banks, and B. Post, *Acta Crystallogr.* **9,** 475 (1956).
4. J. A. Perri, E. Banks, and B. Post, *J. Appl. Phys.* **28,** 1272 (1957).
5. S. Sawada, *Phys. Rev.* **91,** 1010 (1953).
6. I. Lefkowitz, M. B. Dowell, and M. A. Shields, *J. Solid State Chem.* **15,** 24–39 (1975).
7. S. Tanisaki, *J. Phys. Soc. Jpn.* **15,** 566–573 (1960).
8. E. Salje, *J. Appl. Crystallogr.* **7,** 615–617 (1974).
9. B. T. Matthias and E. A. Wood, *Phys. Rev.* **84,** 1255 (1951).
10. R. Le Bihan and C. Vacherand, *J. Phys. Soc. Jpn.* **28,** 159 (1979).
11. R. Gehlig and E. Salje, *Phil. Mag. B* **47,** 229 (1983).
12. E. Salje, in "Polarons and Bipolarons in High T_c Superconductors and Related Materials" (E. K. H. Salje, A. S. Alexandrov, and L. Y. Liang, Eds.), pp. 110–132. Cambridge Univ. Press, Cambridge, 1995.
13. E. Salje, *Ferroelectrics*, **12,** 215–217 (1976).
14. P. M. Woodward, A. W. Sleight, and T. Vogt, *J. Phys. Chem. Solids* **56,** 1305–1315 (1995).
15. D. E. Cox, in " Synchrotron Radiation Crystallography" (P. Coppens, Ed.), pp. 186–254. Academic Press, London, 1992.
16. A. Altomere, M.C. Burla, G. Cascarano, C. Giacovazzo, A. Guagliardi, A. G. G. Moliterni, and G. Polidori, *J. Appl. Crystallogr.* **28,** 842–846 (1995).
17. A. LeBail, H. Duroy, and J. L. Forquet, *Mater. Res. Bull.* **23,** 447–452 (1988).
18. A. Altomere, G. Cascarano, C. Giacovazzo, A. Guagliardi, M. C. Burla, G. Polidori, and M. Camalli, *J. Appl. Crystallogr.* **27,** 435–436 (1994).
19. A. C. Larson and R. B. Von Dreele, "LANSCE." Los Alamos National Laboratory, Los Alamos, NM, 1994.
20. W. C. Hamilton, *Acta Crystallogr.* **18,** 502–510 (1965).
21. A. M. Glazer, *Acta Crystallogr. B* **28,** 3384–3392 (1972).
22. P. M. Woodward, *Acta Crystallogr. B*, in press (1996).
23. T. B. Zunic and I. Vickovic, *J. Appl. Crystallogr.* **29,** 305–306 (1996).
24. P. A. Cox, "The Electronic Structure and Chemistry of Solids." Oxford Univ. Press, Oxford, 1991.
25. R. Hoffman, *J. Chem. Phys.* **39,** 1397–1412 (1963).
26. M.-H. Whangbo and R. Hoffman, *J. Am. Chem. Soc.* **100,** 6093–6098 (1978).
27. R. Hoffman, "Solids and Surfaces: A Chemist's View of Bonding in Extended Structures." VCH Publishers, New York, 1988.
28. G. Miller, "NEW5, Extended Hückel Band Structure Calculation Program." Iowa State University, 1990.
29. R. S. Roth and J. L. Waring, *J. Res. Natl. Bur. Stand.* (*U.S.A*) **70,** 281–303, 1966.
30. J. M. Berak and M. J. Sienko, *J. Solid State Chem.* **2,** 109 (1970).
31. W. L. Kehl, R. G. Hay, and D. Wahl, *J. Appl. Phys.* **23,** 212–215 (1952).
32. E. Salje, *Acta Crystallogr. B* **33,** 547–577 (1977).
33. S. Tanisaki, *J. Phys. Soc. Jpn.* **15,** 573–581 (1960).
34. B. O. Loopstra and H. M. Rietveld, *Acta Crystallogr. B* **25,** 1420–1421 (1969).
35. R. Diehl, G. Brandt, and E. Salje, *Acta Crystallogr. B* **34,** 1105–1111 (1978).